THE JOURNAL OF BIOLOGICAL CHEMISTRY VOL. 289, NO. 21, pp. 15094–15103, May 23, 2014

Dimerization, Oligomerization, and Aggregation of Human Amyotrophic Lateral Sclerosis Copper/Zinc Superoxide Dismutase 1 Protein Mutant Forms in Live Cells*

Received for publication, December 11, 2013, and in revised form, March 26, 2014 Published, JBC Papers in Press, April 1, 2014, DOI 10.1074/jbc.M113.542613

Jiho Kim (김지호)[1], **Honggun Lee** (이홍근)[1], **Joo Hyun Lee** (이주현), **Do-yoon Kwon** (권도윤), **Auguste Genovesio, Denis Fenistein, Arnaud Ogier, Vincent Brondani, and Regis Grailhe**[2]

From Neurodegeneration and Applied Microscopy, Institut Pasteur Korea, Seongnam-Si, Gyeonggi-Do 463-400, Republic of Korea

Background: Copper/zinc superoxide dismutase (SOD1) genetic mutants are associated with familial amyotrophic lateral sclerosis (ALS). Mutant proteins form abnormal aggregates.
Results: We used imaging of live cells to observe SOD1 proteins harboring mutations associated with ALS.
Conclusion: SOD1 mutations impair its dimerization, leading to subsequent aggregation.
Significance: Analysis of the SOD1 quaternary structure in living human cells correlates with previous biochemical data.

More than 100 copper/zinc superoxide dismutase 1 (SOD1) genetic mutations have been characterized. These mutations lead to the death of motor neurons in ALS. In its native form, the SOD1 protein is expressed as a homodimer in the cytosol. *In vitro* studies have shown that SOD1 mutations impair the dimerization kinetics of the protein, and *in vivo* studies have shown that SOD1 forms aggregates in patients with familial forms of ALS. In this study, we analyzed WT SOD1 and 9 mutant (mt) forms of the protein by non-invasive fluorescence techniques. Using microscopic techniques such as fluorescence resonance energy transfer, fluorescence complementation, image-based quantification, and fluorescence correlation spectroscopy, we studied SOD1 dimerization, oligomerization, and aggregation. Our results indicate that SOD1 mutations lead to an impairment in SOD1 dimerization and, subsequently, affect protein aggregation. We also show that SOD1 WT and mt proteins can dimerize. However, aggregates are predominantly composed of SOD1 mt proteins.

ALS is a progressive neurodegenerative disorder caused by the degeneration of motor neurons. Most cases of ALS are sporadic, but ~10% are familial (fALS).[3] One-quarter of fALS cases are inherited because of mutations in the *sod1* gene, which encodes an enzyme responsible for scavenging free radicals (1). The fALS disorder is primarily a heterozygous genetic condition. More than 140 point mutations have been found in the SOD1 peptide sequence. Differences in the *Sod1* gene mutations are associated with variability in the onset and duration of the disease (2). A notable exception is A4V, the mutation that is frequently observed in fALS pedigrees. This mutation is consistently associated with a highly penetrant, early onset, rapidly progressing form of the disease (3). It is widely accepted that the pathology of ALS does not arise from a loss of SOD1 activity (4) but, rather, from a dominant gain of function effect. Although a variety of reasons for this toxicity have been proposed, the structural instability of the SOD1 mt (5) and the presence of SOD1-containing aggregates in neurons (6) as well as in animal models (7) strongly suggest that the observed "aggresomes" are composed of misfolded SOD1 proteins (8) and may play a causal role in the disease.

In vitro studies have shown that the SOD1 mutation carried in fALS patients results in an altered tertiary structure that impairs SOD1 dimer formation (9). Some mutations involve a conformational change that induces protein aggregation as a result of the formation of intermolecular disulfide bonds between the cysteine residues at positions 6 and 111 (10). SOD1 protein ubiquitination is catalyzed by the Dorfin (11) or E6-AP (12) ubiquitin ligases and promotes degradation of specific SOD1 aggregates. It is likely that SOD1 aggregation and ubiquitination are connected because any change in the SOD1 quaternary structure modifies the SOD1-SOD1 interface, thereby affecting the kinetics of dimer formation. It should be noted that *in vitro* study conditions, such as protein concentration and environment, are very different from those that occur *in vivo*. Therefore, in this study, we set out to assess the effects of the SOD1 fALS pathological mutations on dimerization, oligomerization, and aggregation within the cellular context using non-invasive methods. We applied several imaging approaches to study SOD1 dimer formation, namely fluorescence lifetime imaging microscopy (FLIM), fluorescence correlation spectroscopy (FCS), and bimolecular fluorescence complementation (BiFC) (13). We analyzed nine fALS mutations to study SOD1 dimerization. We further showed the formation of aggregates, the colocalization of WT and mt SOD1 proteins, and their cellular diffusion properties. Our results clearly define the effects

* This work was supported by Basic Science Research Program through the National Research Foundation of Korea Grant 2012R1A2004980 funded by the Ministry of Education, Science, and Technology and by National Research Foundation of Korea Grant 2007-00559 funded by the Korean government, the Gyeonggi-do, and Korea Institute of Science and Technology Information (KISTI).

[1] Both authors contributed equally to this work.

[2] To whom correspondence should be addressed: Neurodegeneration and Applied Microscopy, Institut Pasteur Korea, Seongnam-Si, Gyeonggi-Do 463-400, Republic of Korea. Tel.: 82-31-8018-8260; Fax: 82-31-8018-8213; E-mail: regis.grailhe@ip-korea.org.

[3] The abbreviations used are: fALS, familial ALS; mt, mutant; SOD, superoxide dismutase; FLIM, fluorescent lifetime imaging; BiFC, bimolecular fluorescence complementation; FCS, fluorescence correlation spectroscopy; CFP, cyan fluorescent protein; YFP, yellow fluorescent protein; ALLN, acetyl-L-leucyl-L-norleucinal; NA, numerical aperture.

of SOD1 mutations on SOD1 protein dimerization and aggregation in the cellular context.

EXPERIMENTAL PROCEDURES

Plasmid Constructs—Human superoxide dismutase 1 (*sod1*) cDNA (Origene, Abingdon, UK, catalog no. SC111022) was cloned into the mammalian expression vectors pEYFP-C1/N1 and pECFP-C1/N1 (Clontech, BD Biosciences). We used an improved form of CFP that contained an aspartic acid substituted for a histidine residue at position 148, resulting in increased fluorescence lifetime and quantum yield. This modification improved the fluorescence energy transfer when combined with YFP. The *sod1* mutations A4V, G37R, H46R, G85R, D90A, G93A, G93C, I104F, and I113T were generated using PCR-based site-directed mutagenesis (QuikChange® Multi site-directed mutagenesis kit, Stratagene).

The mutant *sod1* derivatives studied in this work were selected by the following criteria. A4V (short survival, 1.4 ± 0.9 years) is located at the dimerization interface and is the most frequent mutation in the United States (3). G37R (long survival) is a gain-of-charge substitution in a β strand (14). H46R is located in a β strand, causes loss of copper binding in the active site of SOD1, and is the most frequent mutation in Japan (long survival, 17.2 ± 7.2 years) (15, 16). G85R (medium survival, 6.0 ± 4.5 years) is a gain-of-charge mutation in a β strand (2). D90A (sensory prodromal for months to years; only homozygous; long survival, 14.2 ± 7.0 years) is a loss-of-charge substitution located at the protein surface (17). G93A (short survival, 2.3 ± 1.5 years) and G93C (long survival) are modifications at a surface-exposed β strand. G93A has been studied extensively because it was the first SOD1 fALS mouse model (18). I104F is a mutation to an aromatic amino acid in an α helix (long survival, 13 ± 1 years) (1), and I113T (which can progress rapidly, 3.6 ± 2.6 years) is a mutation located at the dimerization interface (3). For the BiFC assay, the YFP (1–238) sequences encoding amino acid residues 1–172 (YN172) and 155–238 (YC155) were fused in-frame upstream and downstream of the coding *sod1* sequence, respectively, with a flexible linker sequence (GGGGSGGG). All constructs were confirmed by sequencing.

Cell Culture—HEK 293 cells were maintained in Dulbecco's modified Eagle's medium supplemented with 10% fetal bovine serum, 100 units/ml penicillin, and 0.1 mg/ml streptomycin. Transient transfections with mammalian expression plasmids encoding for the fusion proteins were performed using FuGENE 6 transfection reagent (Roche Applied Science). The cells were cultivated with 10 μg/ml ALLN (Calbiochem) for aggregate quantification.

FLIM—We used FLIM to quantify SOD1 dimerization. The FLIM data were obtained with a Leica TCS SP2 microscope equipped with a FLIM SPC830 module from Becker and Hickl. The fluorescence lifetime profile of HEK 293 cells expressing the CFP proteins was quantified using time-correlated single photon counting. The FRET efficiency was calculated from the lifetime of CFP in the absence and presence of acceptor molecules. The decay profile of CFP was fitted to a single exponential curve according to the monoexponential property of the H148D variant form of CFP (19). Samples coexpressing SOD1 WT and mutant forms tagged with CFP or YFP, respectively, were excited by a pulsed diode laser operated at a repetition rate of 40 MHz at 405 nm. The emitted light was collected through an emission filter set to selectively transmit between 470 and 500 nm. For the statistical analysis, at least 60 cell images were collected for the SOD1 WT and mutant constructs. Importantly, we avoided cell aggregates during this analysis so that we could exclusively quantify SOD1 dimerization. To monitor the fluorescence intensity of the CFP and YFP, we used fixed settings, including laser intensity, photo multiplicator level, and pinhole size. For the statistical analysis, over 30 images were collected for each donor-acceptor combination. The images were analyzed as described previously (20). The correlation between FRET measurements and the ratio of YFP/CFP intensity is reported for each sample of cells analyzed. Because of the experimental setting, the FLIM mean value (in nanoseconds) does not accurately reflect the magnitude of the interaction. The linear regression and variance of the slope was calculated. Because some of the mutant analysis was rejected on the basis of significance (R square <0.3), the values are used to estimate the interaction by comparison with the wild type. Values near 0.00 reflect the absence of interaction and SOD1 dimerization.

Fluorescence Complementation (BiFC)—We established BiFC-stable cell lines expressing constructs encoding WT and mutant forms of SOD1 that were fused to complementary fluorescent protein fragments. These were established by two successive rounds of transfection. First, SOD1 WT and mutant DNA sequences fused to the complementary fluorescent protein fragment were introduced together. As a control for the expression level, we established a cell line constitutively expressing the mCherry protein. Prior to imaging, the transfected cells were incubated at 37 °C for 24 h and then switched to 30 °C for 0–24 h to promote fluorophore maturation. For detection of the BiFC constructs, we used confocal excitation of 488 and 532 nm wavelengths. Emission at 535 nm was detected using a camera. A ×20/0.7 NA water immersion lens was used for these experiments.

Imaging Quantification—To quantify the fluorescence and texture of our images, we used Image Mining, a custom-made image processing and analysis application with an extendable "plug-in" infrastructure (21). The cells were segmented using a sequence of processing steps (22) described previously. Then, on the basis of the cellular segmentation (total intensity), the fluorescence intensity was measured and averaged.

FCS Instrumentation—FCS measurements were performed at room temperature with an FCS extension attached to a Leica TCS SP2 AOBS confocal laser-scanning microscope (Leica Microsystems, Manheim, Germany). For YFP excitation, we used the 514-nm line of the argon laser. The excitation beam was focused onto the sample through an HCX PL Apo CS 63 × 1.2 water immersion objective. The fluorescence was collected by the same objective, separated from the excitation light by a dichroic mirror, and sent onto the avalanche photodiode. The pinhole size was set as 1 airy unit, depending on the objective type for all measurements. The YFP emission was collected selectively through a 535- to 585-nm bandpass filter. Images of single cells expressing each cDNA were taken prior to the actual FCS measurement. The laser beam was then focused at a selected spot within the cytoplasm, and FCS measurements

were taken for 100 s. The autocorrelation curves were acquired, processed, and evaluated using the Leica/ISS FCS software.

FCS Data Analysis—The autocorrelation function, G(τ), for the FCS experiment was calculated from the photon counts using Equation 1,

$$G(\tau) = \frac{< \delta F(t) \cdot \delta F(t+\tau) >}{< F(t) >^2} \quad \text{(Eq. 1)}$$

where, $F(t)$ represents the detected photon counts at time t, which is the lag time. The angle brackets represent the time average. The normal three-dimensional diffusion could be fitted using Equation 2,

$$G(\tau) = 1 + \frac{1}{N}\left(1 + \frac{\tau}{\tau_D}\right)^{-1} \cdot \left(1 + S^2 \cdot \frac{\tau}{\tau_D}\right)^{-\frac{1}{2}} \quad \text{(Eq. 2)}$$

where N is the average number of fluorescent particles in the observation volume defined by the radius, r_o, and length, $2z_o$, and S is the structure parameter representing the ratio (r_o/z_o). The diffusion time of YFP expressed in the HEK 293 cell as a standard sample and the characteristic diffusion time were determined to be ~500 μs, which is ~10 times slower than in solution.

RESULTS

Analysis of SOD1 Complexes Using YFP/CFP FRET and FLIM—To analyze SOD1 dimerization properties in live cells, we developed a FRET strategy by fusing SOD1 proteins to the N or C termini of CFP and YFP, coexpressed them, and used FLIM to quantify interactions between SOD1 protein monomers. Our approach allowed us to discriminate between the CFP fluorescence and the FRET signal (Fig. 1*A*). The SOD1 dimer proteins, including the WT and/or G93A mutant form, are depicted in Fig. 1*B*.

To confirm that the WT SOD1-expressing cells used for the FRET analysis did not contain SOD1 aggregates in their cytosol, we analyzed cells expressing only the C-terminal SOD1-CFP fusion as a negative control (Fig. 1*B*, *Control*). The results (Fig. 1*B*, *bottom panel*), presented as lifetime (nanoseconds), show that the strongest FRET signal was obtained in cells expressing the N-terminal/C-terminal SOD1 fusion protein (Fig. 1*B*, *(3)*). We observed a FRET signal with the WT SOD1 protein but not with the G93A mutant and the negative control. Fig. 1*C* shows that the WT protein (*left panel*) has a shorter lifetime distribution in the cell than the G93A mt protein (*right panel*). We also observed that the lifetime signature of the SOD1 protein-protein interaction was distributed homogenously in all cells without visible aggregation, suggesting that the SOD1 WT protein had formed dimers.

We subsequently performed single-cell lifetime fluorescence quantification *versus* YFP/CFP fluorescence intensity for SOD1 WT and G93A mutant forms (Fig. 2*A*). The SOD1 WT protein showed a clear decrease in its fluorescence lifetime according to the relative concentration of the SOD1-YFP acceptor, indicating SOD1 interaction. In contrast, we detected no change in the lifetime of the SOD1 93A mutant compared with the SOD1-YFP acceptor. This absence of FRET indicated that the SOD1 93A mutant failed to dimerize. We then analyzed nine SOD1 mutant proteins clinically associated with fALS by lifetime fluorescence quantification intensity (Fig. 2*B*). The mutations were chosen for their variable clinical and biochemical effects and for their positions in the SOD1 high-resolution, three-dimensional crystal structure. The A4V mutant amino acid residue, which is located at the dimerization interface and is known to reduce SOD1 dimerization by steric effects, showed a FRET pattern similar to that observed for the G93A mutant. A second mutation at the dimerization interface, I113T, does not have a strong steric effect and showed a moderate distribution and lower FRET than the WT SOD1 protein. Finally, the H46R mutant, which mediates copper binding at the active site in the core protein, showed an intermediate distribution between the WT and the G93A mutant control. Other mutations we analyzed showed a pattern similar to that of the control G93A mutant, indicating a SOD1 interaction defect.

SOD1 Dimerization Defect in Homodimer and Heterodimer Complexes—To study SOD1 dimerization in live cells, we performed BiFC, a useful tool for analyzing molecular interactions at the cellular level. It entails fusing two fragments of a fluorescent protein, each of which cannot fluoresce independently, to proteins to be tested for interactions. When the proteins of interest interact, a functional fluorochrome is reassembled that is detected by restoration of a fluorescent signal. To test for SOD1 dimerization, we fused SOD1 polypeptides with the yellow fluorescence protein fragments YN172 (A) and YC155 (B). The YN172 and YC155 fragments were fused to the WT and G93A mutant SOD1 proteins at the C terminus (SOD1-A or SOD1-B) and N terminus (A-SOD1 or B-SOD1). Because the SOD1 protein forms homodimers, we tested several variations of homodimers, including SOD1-A/SOD1-A, SOD1-B/SOD1-B, and SOD1-A/SOD1-B. However, only the A/B combination homodimer restored YFP fluorescence (Fig. 3*A*).

We then expressed the four possible combinations (Fig. 3*B*, *top panel*) and measured the restored fluorescence complementation that occurred upon SOD1 dimerization (Fig. 3*B*, *bottom panel*). No fluorescence was detected for combinations 2 and 4 in Fig. 3*B* or for the negative control expressing only YN172 and YC155 (Fig. 3*B*, *Control*). However, we found that combinations 1 and 3 in Fig. 3*B* yielded high fluorescence signals. For both combinations, there was a reduction in the fluorescence intensity for the G93A mutant compared with the WT protein. As depicted in Fig. 3*C*, the confocal images of the WT and G93A mt combination (1) indicated a homogeneous distribution of the proteins and no alterations in cellular morphology. We did not observe SOD1 aggregates in cells expressing a combination (1). However, some aggregations were detected in cells expressing a combination (3) (data not shown). Hence, we chose to use a combination (1) to study SOD1 protein dimerization.

Because fALS disease is caused by heterozygotic mutations at the *sod1* locus, we next used BiFC to analyze a combination of WT and mutant SOD1 proteins. As shown in Fig. 4*A*, we examined three different SOD1 BiFC conditions, including WT and mutant homodimers and WT/mutant heterodimers. The BiFC approach allows us to measure WT/mutant heterodimer formation independently of homodimers, although all forms are present in cells of fALS patients. The dimers formed between

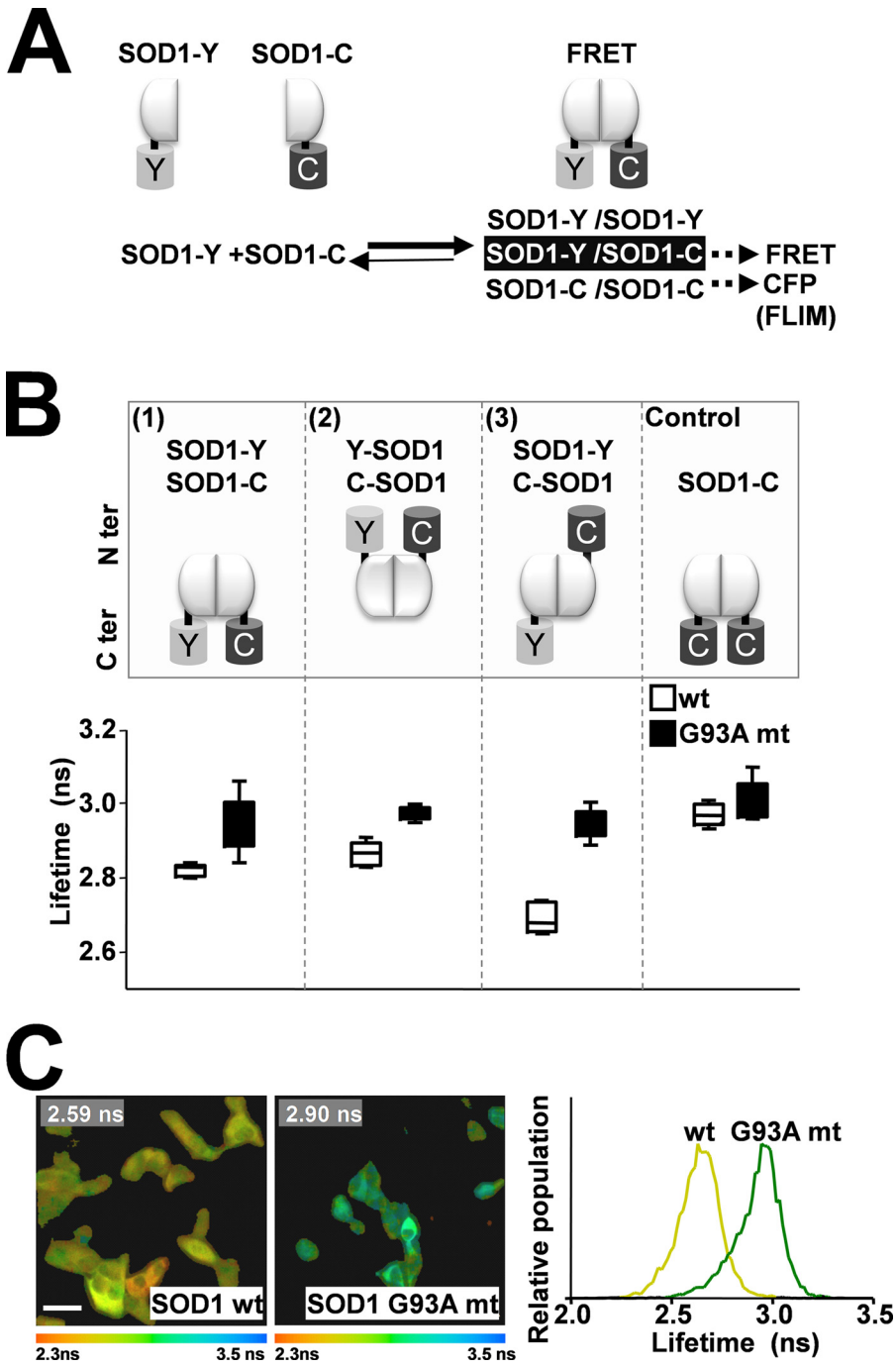

FIGURE 1. **FRET and fluorescence lifetime analysis of SOD1 proteins in living cells.** *A*, SOD1 protein dimerization and FRET analysis. Shown is a schematic of SOD1 dimerization and fluorescence of YFP and CFP fusion proteins. *B*, analysis of three combinations (*1*, *2*, and *3*) of YFP- and CFP-tagged WT and G93A mutant SOD1 fluorescent pairs ($n = 5$). *C*, FLIM visualization of the degree of donor fluorophore lifetime shortening on a pseudocolor scale. The color-coded FLIM images show the WT and G93A mutant. The average fluorescence lifetimes of the WT and G93A mutant SOD1 homodimers are 2.59 ns and 2.90 ns, respectively. The fluorescence lifetime distribution of the CFP- and YFP-tagged SOD1 proteins is shown.

WT and G93A mutant SOD1 monomers showed an intermediate fluorescence signal. The measured values indicate homodimers comprised of WT and mt SOD1 proteins (Fig. 4*B*). We then quantified the YFP fluorescence signal for all of the mutant SOD1 homodimers (mutant SOD1-A/mutant SOD1-B) and mutant/WT SOD1 heterodimers (WT SOD1-A/mutant SOD1-B). We found that all mutations tested in this study, with the exception of D90A, resulted in the reduction of SOD1 dimerization. As observed previously for the G93A mutant, most of the SOD1 WT/mutant dimers showed intermediate signals compared with the WT and mutant dimers. Interestingly, among the studied mutations located at the dimerization interface, the WT SOD1 subunit was able to form dimers with the I113T, but not with the A4V, mutant.

Association of SOD1 fALS Mutations with Protein Aggregation—The fALS-associated mutation of SOD1 has been shown to promote protein aggregates that are then degraded by the ubiquitination and proteasome pathways. To analyze the formation of

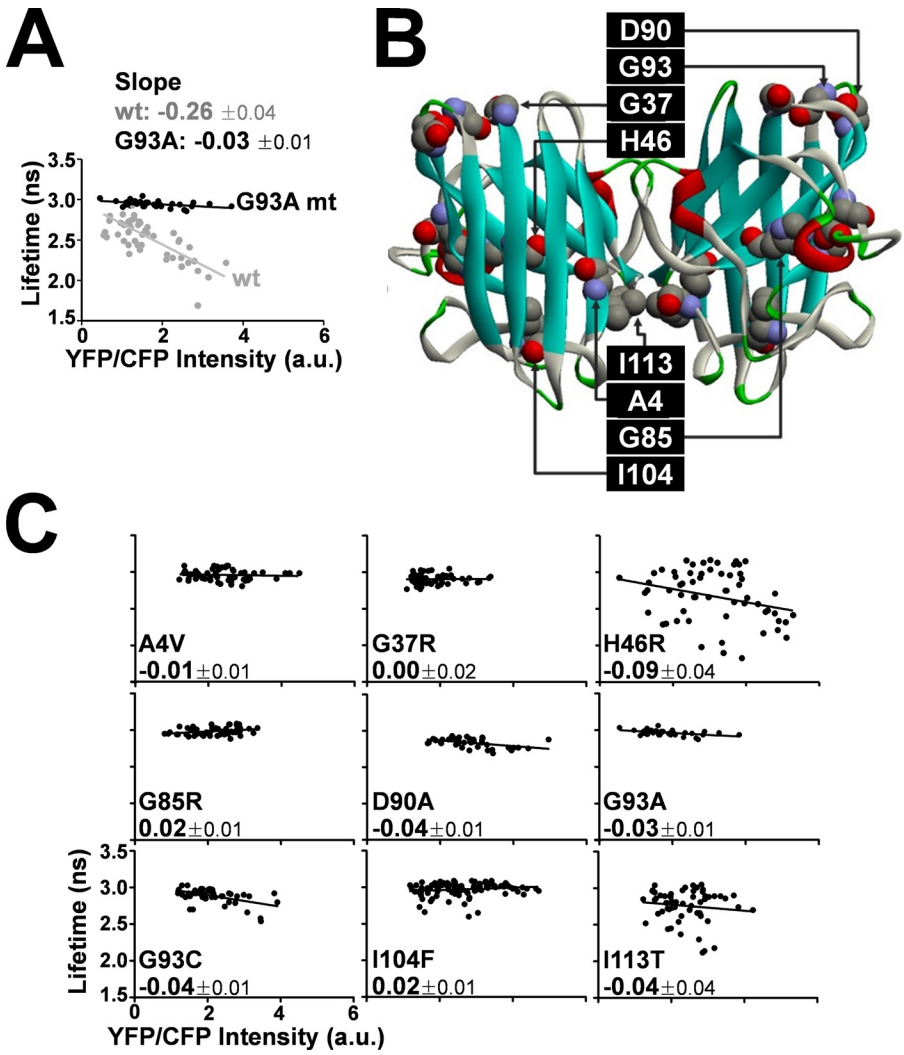

FIGURE 2. **FRET analysis of WT and SOD1 mutant proteins.** *A*, comparison of WT and G93A mutant by FRET analysis (number of cells analyzed, $n = 60$; arbitrary unit, a.u.). *B*, structure of the human SOD1 dimer showing the positions of the fALS mutations. *C*, analysis of the nine selected fALS-associated mutants (number of cells analyzed, $n = 60$).

SOD1 cellular aggregates, we generated stable cell lines expressing the G93A mutant and WT SOD1 proteins fused to CFP and YFP, respectively, and selected for further study a cell line that equally expressed the mutant and WT SOD1 fluorescently tagged constructs. The SOD1 G93A mutant protein, detected in the CFP channel, was distributed as a single fluorescence spot in each cell (Fig. 5*A*, *left panel*). In contrast, the WT SOD1 protein, detected in the YFP channel, was distributed homogeneously (Fig. 5*A*, *right panel*). Fluorescence quantification of a single cell containing the SOD1 G93A mutant further confirmed that the SOD1 mutant protein is the predominant form present in the aggregates (Fig. 5*B*).

To confirm that the WT protein did not generate aggregates, we prevented the SOD1 degradation by using a proteasome inhibitor (ALLN). The WT and G93A mutant spots were quantified under increasing ALLN concentrations (Fig. 5*C*), as reported in previous SOD1 aggregation studies (11, 12). As expected, the number of fluorescent spots for the G93A mt increased as the ALLN concentration increased. However, detection of the spot was negligible for the WT SOD1. At the highest concentration of ALLN, the WT spot detection did not reach the baseline spot formation of the G93A mt.

To study the process of aggregation, we performed time-lapse microscopy on a cell line stably expressing the G93A mutant. The cell line was maintained at 37 °C in a humidified atmosphere with 5% CO_2, and *epi*-fluorescence microscopy images were acquired every 5 min for a period of 18 h. As seen in Fig. 6*A*, the aggregates appeared simultaneously at multiple sites of the cells and grew over a period of minutes before fusing together, thereby generating larger aggregates, and converging into a single spot. The aggregates did not form at specific sites within the cell.

We next analyzed the aggregation of the nine mutant fALS-related SOD1 proteins. Cells were transiently transfected in the presence and absence of ALLN, visualized after 48 h, and then protein aggregation was quantified (Fig. 6*B*). Under these experimental conditions, we observed aggregates in cells expressing all the tested mutant proteins except for I113T, D90A, and H46R. In the presence of the ALLN proteasome inhibitor, we detected an increase in the number of cells with

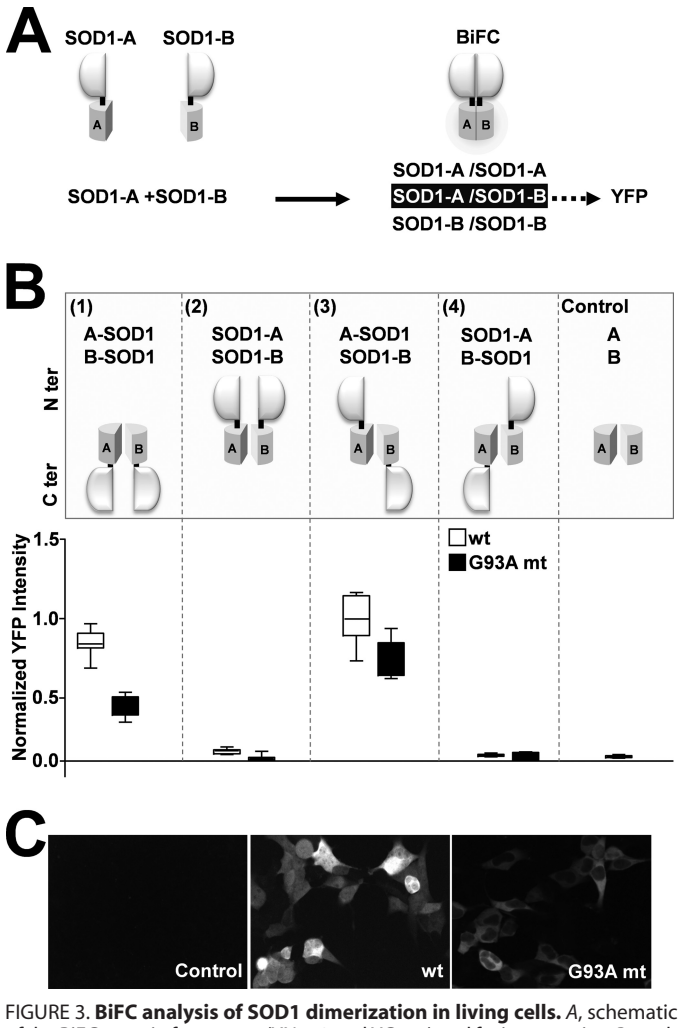

FIGURE 3. **BiFC analysis of SOD1 dimerization in living cells.** *A*, schematic of the BiFC protein fragments (YN172 and YC155) and fusion proteins. *B*, analysis of four combinations (*1*, *2*, *3*, and *4*) of SOD1 WT and G93A mutant proteins ($n = 3$). *C ter*, C terminus; *N ter*, N terminus. *C*, BiFC confocal image of control, WT, and G93A mutant cells observed using combination 1.

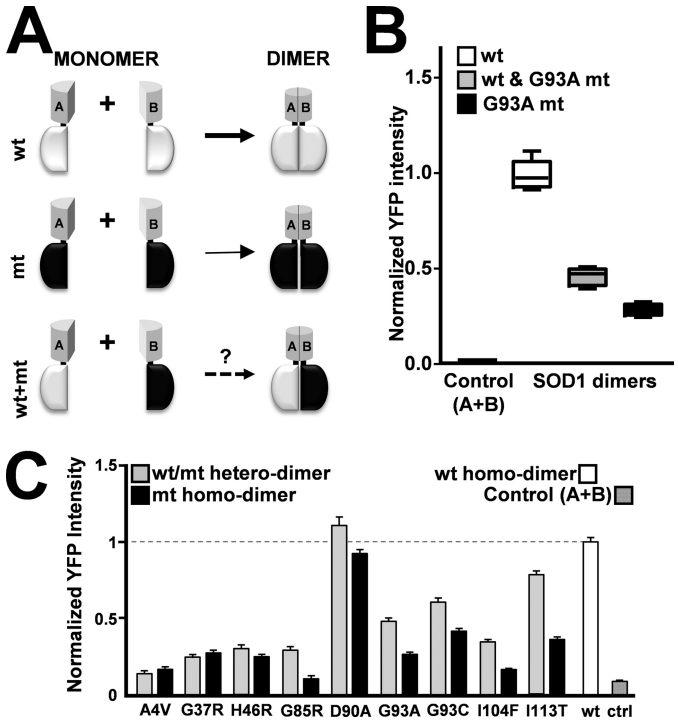

FIGURE 4. **BiFC analysis of SOD1 mutant and WT-mutant heterodimers.** *A*, schematic of the BiFC WT and mutant combinations. *B*, BiFC analysis of the WT and G93A mutant homodimers and the WT/G93A mutant heterodimer ($n = 3$). *C*, histogram representation of the results obtained for the WT, mutant, and WT/mutant dimers ($n = 3$).

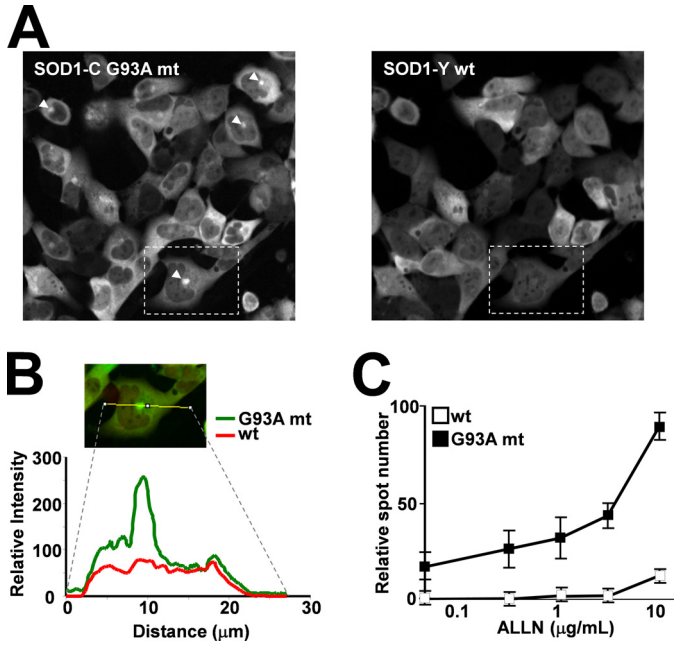

FIGURE 5. **Fluorescence analysis of cells stably coexpressing fluorescent WT and G93A mutant SOD1 proteins.** *A*, image of the cell line stably expressing WT (SOD1-Y WT) and G93A mutant (SOD1-C G93A) fused to YFP and CFP, respectively. The *arrows* indicate the positions of aggregates. *B*, analysis of YFP and CFP fluorescence in a cell with SOD1 aggregates. *C*, effect of ALLN proteasome inhibitor concentration on the number of fluorescent spots detected in WT or G93A mutant SOD1-expressing cells ($n = 5$).

cellular aggregates for all SOD1 mutant proteins except for H46R.

Cellular Diffusion of Fluorescent SOD1 G93A Mutant Compared with Wild-type Protein—Although we showed that the fALS-related SOD1 mt proteins displayed a loss in their ability to homodimerize and an increase in aggregation, we also wanted to examine the intermediate multimeric state of SOD1. To study the assembly of mutant forms of SOD1, we employed a microscopic technique called FCS that is capable of measuring the mobility of a single molecule by tracking its fluorescent signature in one targeted locus of living cells. We used FCS to measure, in living cells, the correlation time (τ_D) of fluorescently tagged proteins, which is related to the diffusion coefficient and the molecular weight of the protein complex. We analyzed two cell lines expressing either the WT and or G93A mutant protein fused to YFP. For the G93A mutant, we compared cells with or without aggregates (Fig. 7). We observed that the WT protein, but not G93A mutant, could be distinguished from the native YFP (Fig. 7, *Control*). However, the diffusion time for the G93A mutant in cell with no visible aggregates was reduced compared with that of the WT protein, which is due to the size difference between the SOD1 WT and mutant proteins that are in dimeric and monomeric states, respectively. The cells expressing the G93A mutant contained

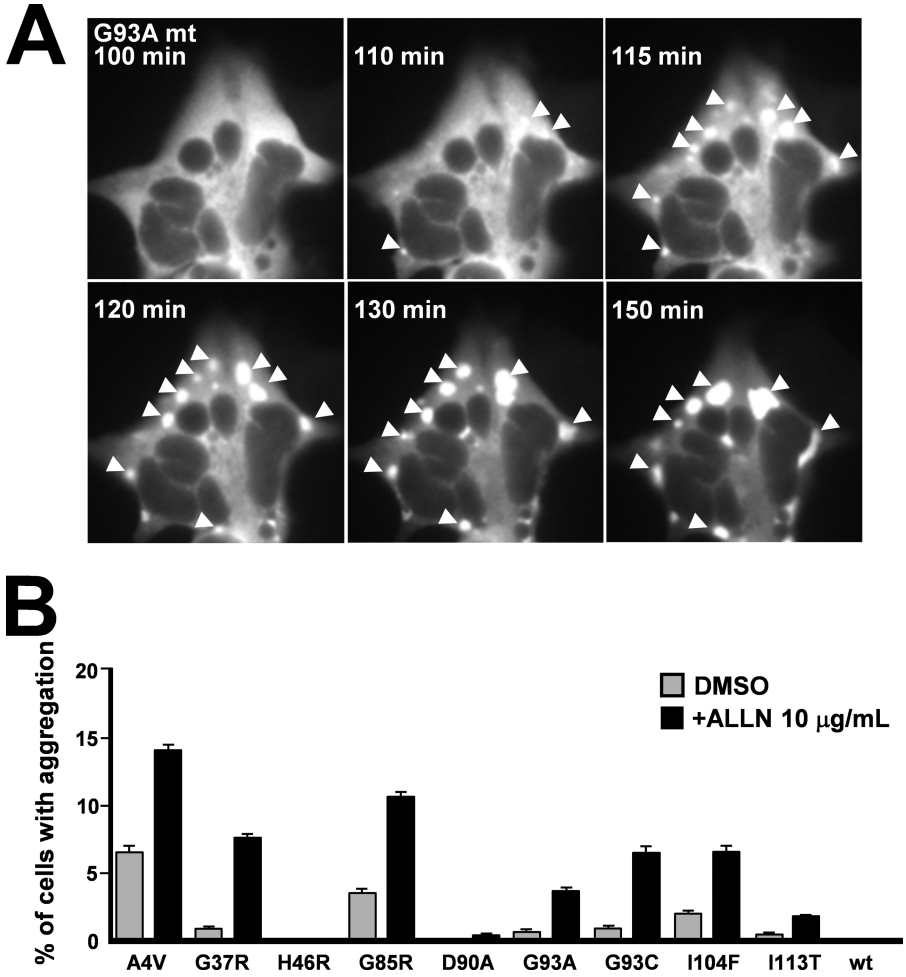

FIGURE 6. **Analysis of mutant SOD1 aggregation in living cells.** *A*, time course analysis of G93A mt aggregation in a single cells. The *arrows* indicate the positions of the aggregates. *B*, histogram representation of the percentage of cells showing aggregates in cell culture expressing mutant SOD1 proteins with or without the ALLN proteasome inhibitor. *DMSO*, dimethyl sulfoxide.

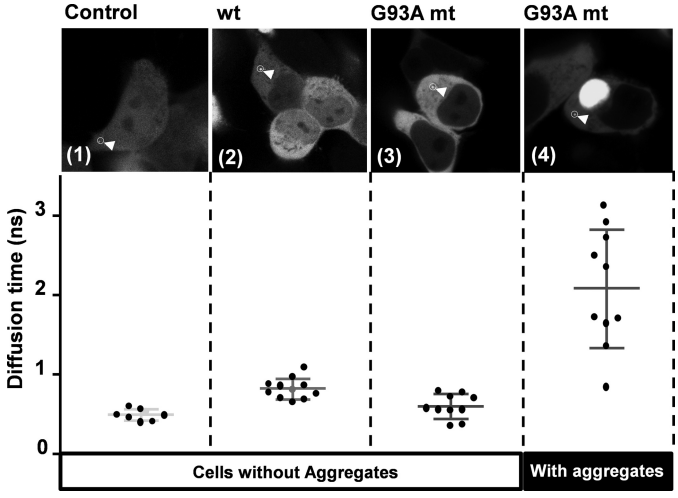

FIGURE 7. **Analysis of WT and G93A mutant SOD1 protein diffusion in living cells.** *Top panels*, typical analyzed cells. The *arrows* indicate the position of fluorescence diffusion detection. *Bottom panels*, plots of the quantification of the diffusion times for several cells.

aggregates with high diffusion time values and variance between cells that likely represent SOD1 at various degrees of oligomerization.

DISCUSSION

Among the SOD1 mutations analyzed, we studied mutations that directly affect the dimerization interface (A4V and I113T) and mutations spread across the β sheet secondary structures (G37R, H46R, G85R, D90A, G93A, G93C, and I104F). Using FRET and BiFC, we found that SOD1 dimerization in living cells was consistently reduced for most of these mutant proteins. It should be noted that these techniques required modification of the SOD1 protein by tagging it with fluorescent proteins or fragments for the FRET and BiFC techniques, respectively.

The combination of our results with structural data suggests that defective dimerization of the SOD1 mutants is due to altered tertiary structures. FRET analysis of the mutant proteins showed that, for H46R and I113T, homodimerization was disrupted but remained more discrete. The His-46 amino acid is involved in the copper-zinc binding site. Interestingly, the H46R mutation showed a moderate effect on dimerization by FRET. One could conclude that the H46R phenotype is due to the loss of the copper-zinc binding site and a moderate defect in dimer formation. These quantitative results obtained for typical mutations corroborate the clinical data currently available. In fact, the A4V mutant, which drastically affected SOD1

A

	*Survival (years)	*ΔΔG (kcal/mol)	FRET (Slope)	BiFC (Homodimer)	BiFC (Heterodimer)	Aggregat (%) -ALLN	Aggregat (%) +ALLN
WT	ND	ND	−0.26 ±0.04	1.00 ±0.00	ND	0.00 ±0.00	0.00 ±0.00
A4V	1.4 ±0.9	-4.31	−0.01 ±0.01	0.16 ±0.02	0.15 ±0.02	6.59 ±0.38	14.09 ±0.54
G37R	ND	ND	0.00 ±0.02	0.25 ±0.03	0.26 ±0.01	0.89 ±0.13	7.63 ±0.33
H46R	17.2 ±7.2	0.48	−0.09 ±0.04	0.26 ±0.03	0.31 ±0.01	0.02 ±0.02	0.01 ±0.01
G85R	6.0 ±4.5	-0.90	0.02 ±0.01	0.12 ±0.00	0.34 ±0.02	3.66 ±0.23	10.60 ±0.53
D90A	14.2 ±7.0	-0.65	−0.04 ±0.01	0.90 ±0.07	1.12 ±0.14	0.12 ±0.05	0.18 ±0.05
G93A	2.3 ±1.5	-2.98	−0.03 ±0.01	0.26 ±0.02	0.50 ±0.04	0.76 ±0.11	3.80 ±0.22
G93C	10.1 ±6.0	ND	−0.04 ±0.01	0.41 ±0.04	0.64 ±0.39	0.96 ±0.10	6.38 ±0.51
I104F	13.0 ±1.0	-1.24	0.02 ±0.01	0.18 ±0.01	0.34 ±0.03	2.05 ±0.19	6.57 ±0.57
I113T	3.6 ±2.6	-2.48	−0.04 ±0.04	0.36 ±0.03	0.82 ±0.04	0.07 ±0.03	1.77 ±0.16

B

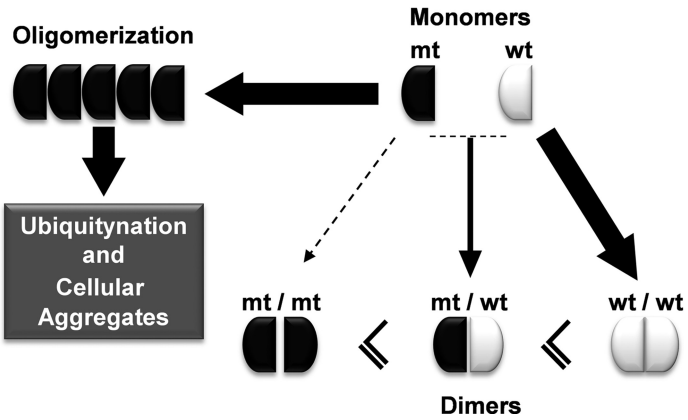

FIGURE 8. **Cellular models of cellular SOD1 protein analysis.** *A*, summary of quantitative measurement on WT and mutant SOD1 proteins. **Survival* and *ΔΔ*G* are experimental results from Refs. 5, 9. *ND*, not determined. *B*, molecular model of the cellular distributions of WT and fALS mutant SOD1.

dimerization, has been shown to have a dramatic effect on patients and is associated with rapid disease progression. As expected, on the basis of the data showing moderate effects on dimerization, the H46R and I113T mutations are associated with longer disease onset than that associated with the A4V mutation. In addition, the other mutations associated with intermediate disease onset analyzed in this study show dimerization defects that correlate with the clinical observations.

Among the nine mutations tested, we found one mutant form that displayed a discrepancy between the FRET and BiFC techniques. The mutation D90A significantly decreased the SOD1 dimer formation measured by FRET but not by BiFC. One possible explanation for this discrepancy is that the fusion protein used in the BiFC analysis modified the complex association/dissociation dynamics of dimerization, leading to an irreversibly dimerized state. Hence, the D90A mutation may affect only dissociation of the monomers, which cannot be examined by the BiFC approach.

Because fALS is a genetic disease that is usually caused by heterozygous mutations, we performed a quantitative analysis of SOD1 WT/mutant heterodimers. The BiFC technique was selected to quantify SOD1 WT/mutant formation because the FRET technique cannot quantitatively distinguish SOD1 WT/mutant from SOD1 mutant/mutant dimers. As reported previously and as shown using high resolution x-ray crystallography of SOD1, the mutations A4V and I113T affect the dimerization interface (23, 24). The strong dimerization impairment observed by BiFC for the A4V mutant compared with I113T further validates our experimental conditions. Interestingly, the A4V mutation prevented the formation of any SOD1 dimers, whereas the I113T mutation prevented formation of mutant homodimers but allowed formation of WT/mutant heterodimers.

In addition to studying the properties of SOD1 protein dimerization, we also quantified the aggregation of SOD1 WT and mutant YFP fusion proteins in living cells. Under our

experimental conditions, cellular aggregates were observed for almost all of the studied mutations. Key information available to date (clinical, biochemical, FRET, BiFC, and aggregation data) relating to WT and mutant SOD1 proteins are summarized in Fig. 8*A*. Interestingly, we found that the H46R and I113T mutations, which showed a mild effect on dimer formation by FRET analysis, did not produce aggregates when expressed in cells. The D90A mutation, which is associated with mild and late disease onset, did not produce aggregation in our experiments. The A4V mutation had the most drastic dimerization defect and also showed the strongest SOD1 aggregation activity.

By studying SOD1 aggregation using time-lapse microscopy, we found that SOD1 aggregation formation occurs in a relatively short period of time (on the order of a few minutes) and that multiple aggregates form in parallel from various subcytosolic locations. In cells containing aggregates, the diffusion properties of the G93A mutant protein indicated that SOD1 proteins freely diffusing in the cytosol were multimers containing more than two SOD1 monomers. Interestingly, cells expressing the G93A mutant that do not show aggregates contained SOD1 as monomers or dimers. These results suggest that the monomer is the major form of SOD1 associated with fALS prior to the formation of aggregates. The triggering event leading from oligomerization to aggregation remains to be elucidated and will require a greater understanding of the cellular homeostasis of mutant and WT forms of SOD1. Interestingly, the proteasome inhibitor ALLN had a strong impact on SOD1 aggregation, suggesting that SOD1 aggregates are subject to proteasomal degradation.

On the basis of our results, we propose the model shown in Fig. 8*B*. In this model, the SOD1 WT proteins exist primarily as dimers, whereas SOD1 mutant proteins are mostly monomeric. However, we found that the dimer/monomer ratio is variable and dependent upon the mutation site. Oligomer formation involves covalent disulfide bonds (C6-C111) between SOD1 monomers (25) that are much more stable (and appear to be irreversible in a cellular context) than the dimerization interaction. We observed that only the SOD1 mutants we studied led to the formation of aggregates, and this process seems to be initiated by SOD1 monomers. The aggregates were composed only of mutant SOD1, and the cellular ubiquitination and proteasome protein degradation machinery was insufficient to prevent the formation of aggregates in our cellular models.

REFERENCES

1. Abe, K., Aoki, M., Ikeda, M., Watanabe, M., Hirai, S., and Itoyama, Y. (1996) Clinical characteristics of familial amyotrophic lateral sclerosis with Cu/Zn superoxide dismutase gene mutations. *J. Neurol. Sci.* **136,** 108–116
2. Rosen, D. R. (1993) Mutations in Cu/Zn superoxide dismutase gene are associated with familial amyotrophic lateral sclerosis. *Nature* **364,** 362
3. Rosen, D. R., Bowling, A. C., Patterson, D., Usdin, T. B., Sapp, P., Mezey, E., McKenna-Yasek, D., O'Regan, J., Rahmani, Z., and Ferrante, R. J. (1994) A frequent Ala 4 to Val superoxide dismutase-1 mutation is associated with a rapidly progressive familial amyotrophic lateral sclerosis. *Hum. Mol. Genet.* **3,** 981–987
4. Bowling, A. C., Barkowski, E. E., McKenna-Yasek, D., Sapp, P., Horvitz, H. R., Beal, M. F., and Brown, R. H., Jr. (1995) Superoxide dismutase concentration and activity in familial amyotrophic lateral sclerosis. *J. Neurochem.* **64,** 2366–2369
5. Lindberg, M. J., Tibell, L., and Oliveberg, M. (2002) Common denominator of Cu Zn superoxide dismutase mutants associated with amyotrophic lateral sclerosis: decreased stability of the apo state. *Proc. Natl. Acad. Sci. U.S.A.* **99,** 16607–16612
6. Matsumoto, G., Stojanovic, A., Holmberg, C. I., Kim, S., and Morimoto, R. I. (2005) Structural properties and neuronal toxicity of amyotrophic lateral sclerosis-associated Cu/Zn superoxide dismutase 1 aggregates. *J. Cell Biol.* **171,** 75–85
7. Puttaparthi, K., Wojcik, C., Rajendran, B., DeMartino, G. N., and Elliott, J. L. (2003) Aggregate formation in the spinal cord of mutant SOD1 transgenic mice is reversible and mediated by proteasomes. *J. Neurochem.* **87,** 851–860
8. Johnston, J. A., Ward, C. L., and Kopito, R. R. (1998) Aggresomes: a cellular response to misfolded proteins. *J. Cell Biol.* **143,** 1883–1898
9. Lindberg, M. J., Byström, R., Boknäs, N., Andersen, P. M., and Oliveberg, M. (2005) Systematically perturbed folding patterns of amyotrophic lateral sclerosis (ALS)-associated SOD1 mutants. *Proc. Natl. Acad. Sci. U.S.A.* **102,** 9754–9759
10. Niwa, J., Yamada, S., Ishigaki, S., Sone, J., Takahashi, M., Katsuno, M., Tanaka, F., Doyu, M., and Sobue, G. (2007) Disulfide bond mediates aggregation, toxicity, and ubiquitylation of familial amyotrophic lateral. *J. Biol. Chem.* **282,** 28087–28095
11. Niwa, J., Ishigaki, S., Hishikawa, N., Yamamoto, M., Doyu, M., Murata, S., Tanaka, K., Taniguchi, N., and Sobue, G. (2002) Dorfin ubiquitylates mutant SOD1 and prevents mutant SOD1-mediated neurotoxicity. *J. Biol. Chem.* **277,** 36793–36798
12. Mishra, A., Maheshwari, M., Chhangani, D., Fujimori-Tonou, N., Endo, F., Joshi, A. P., Jana, N. R., and Yamanaka, K. (2013) E6-AP association promotes SOD1 aggresomes degradation and suppresses toxicity. *Neurobiol. Aging* **34,** 1310
13. Hu, C. D., Chinenov, Y., and Kerppola, T. K. (2002) Visualization of interactions among bZIP and Rel family proteins in living cells using bimolecular fluorescence complementation. *Mol. Cell.* **9,** 789–798
14. Borchelt, D. R., Lee, M. K., Slunt, H. S., Guarnieri, M., Xu, Z. S., Wong, P. C., Brown, R. H., Jr., Price, D. L., Sisodia, S. S., and Cleveland, D. W. (1994) Superoxide dismutase 1 with mutations linked to familial amyotrophic lateral sclerosis possesses significant activity. *Proc. Natl. Acad. Sci. U.S.A.* **91,** 8292–8296
15. Corson, L. B., Strain, J. J., Culotta, V. C., and Cleveland, D. W. (1998) Chaperone-facilitated copper binding is a property common to several classes of familial amyotrophic lateral sclerosis-linked superoxide dismutase mutants. *Proc. Natl. Acad. Sci. U.S.A.* **95,** 6361–6366
16. Aoki, M., Ogasawara, M., Matsubara, Y., Narisawa, K., Nakamura, S., Itoyama, Y., and Abe, K. (1994) Familial amyotrophic lateral sclerosis (ALS) in Japan associated with H46R mutation in Cu/Zn superoxide dismutase gene: a possible new subtype of familial ALS. *J. Neurol. Sci.* **126,** 77–83
17. Andersen, P. M., Nilsson, P., Ala-Hurula, V., Keränen, M. L., Tarvainen, I., Haltia, T., Nilsson, L., Binzer, M., Forsgren, L., and Marklund, S. L. (1995) Amyotrophic lateral sclerosis associated with homozygosity for an Asp90Ala mutation in CuZn-superoxide dismutase. *Nat. Genet.* **10,** 61–66
18. Tu, P. H., Raju, P., Robinson, K. A., Gurney, M. E., Trojanowski, J. Q., and Lee, V. M. (1996) Transgenic mice carrying a human mutant superoxide dismutase transgene develop neuronal cytoskeletal pathology resembling human amyotrophic lateral sclerosis lesions. *Proc. Natl. Acad. Sci. U.S.A.* **93,** 3155–3160
19. Bastiaens, P. I., and Squire, A. (1999) Fluorescence lifetime imaging microscopy: spatial resolution of biochemical processes in the cell. *Trends Cell Biol.* **9,** 48–52
20. Kim, J., Lee, J., Kwon, D., Lee, H., and Grailhe, R. (2011) A comparative analysis of resonance energy transfer methods for Alzheimer related protein-protein interactions in living cells. *Mol. Biosyst.* **7,** 2991–2996
21. Dorval, T., Ogier, A., Genovesio, A., Lim, H. K., Kwon do, Y., Lee, J. H., Worman, H. J., Dauer, W., and Grailhe, R. (2010) Contextual automated 3D analysis of subcellular organelles adapted to high-content screening. *J. Biomol. Screen.* **15,** 847–857

22. Fenistein, D., Lenseigne, B., Christophe, T., Brodin, P., and Genovesio, A. (2008) A fast, fully automated cell segmentation algorithm for high-throughput and high-content screening. *Cytometry A* **73,** 958–964
23. Hough, M. A., Grossmann, J. G., Antonyuk, S. V., Strange, R. W., Doucette, P. A., Rodriguez, J. A., Whitson, L. J., Hart, P. J., Hayward, L. J., Valentine, J. S., and Hasnain, S. S. (2004) Dimer destabilization in superoxide dismutase may result in disease-causing properties: structures of motor neuron disease mutants. *Proc. Natl. Acad. Sci. U.S.A.* **101,** 5976–5981
24. Khare, S. D., and Dokholyan, N. V. (2006) Common dynamical signatures of familial amyotrophic lateral sclerosis-associated structurally diverse Cu, Zn superoxide dismutase mutants. *Proc. Natl. Acad. Sci. U.S.A.* **103,** 3147–3152
25. Banci, L., Bertini, I., Boca, M., Calderone, V., Cantini, F., Girotto, S., and Vieru, M. (2009) Structural and dynamic aspects related to oligomerization of apo SOD1 and its mutants. *Proc. Natl. Acad. Sci. U.S.A.* **106,** 6980–6985